Collagen and Leather

RESEARCH

Open Access

High performance strain sensor based on leather activated by micro-cracking conductive layer

Jianzhong Ma[1,2*], Zhijie Cheng[1,2], Sha Tan[1,2], Tian Zheng[3] and Yan Zong[1,2*]

Abstract

Flexible strain sensors are capable to detect external force induced strain change owing to their unique ability to convert deformation into electrical signals. Generally, micro/nano patterning of conductive layer in strain sensor is an effective method to improve its sensitivity, however the sophisticated manipulation process is limited only in laboratory scale. In this report, a simple and scalable fabrication strategy was used to create micro-cracking conductive layer as an alternative patterning method to achieve high performance of strain sensor. In details, the sensor was fabricated using leather as the substrate to filtrated acidified multi-walled carbon nanotubes (a-MWCNTs)/layered double hydroxides (LDHs) suspension. During stretching process, micro-cracking structure emerged on the percolated a-MWCNTs/LDHs layer, causing a rise up of resistance according to increasing strain and generated a detectable electrical signal. The prepared sensor had a large detecting range (60%), high sensitivity (GF of 7238.92 at strain 30–60%), fast response (tensile response time of 270 ms), good stability and repeatability. The sensor also inherited the advantages of leather, such as biodegradability and good air permeability, and the introduction of a-MWCNTs/LDHs further enhanced its fire retardancy properties. These features ensured the sensor as an eco-friendly, comfortable and safe electronic device for human motion detection.

Keywords a-MWCNTs, LDHs, Leather, Flexible strain sensor

*Correspondence:
Jianzhong Ma
majz@sust.edu.cn
Yan Zong
yzong@sust.edu.cn
Full list of author information is available at the end of the article

Graphical abstract

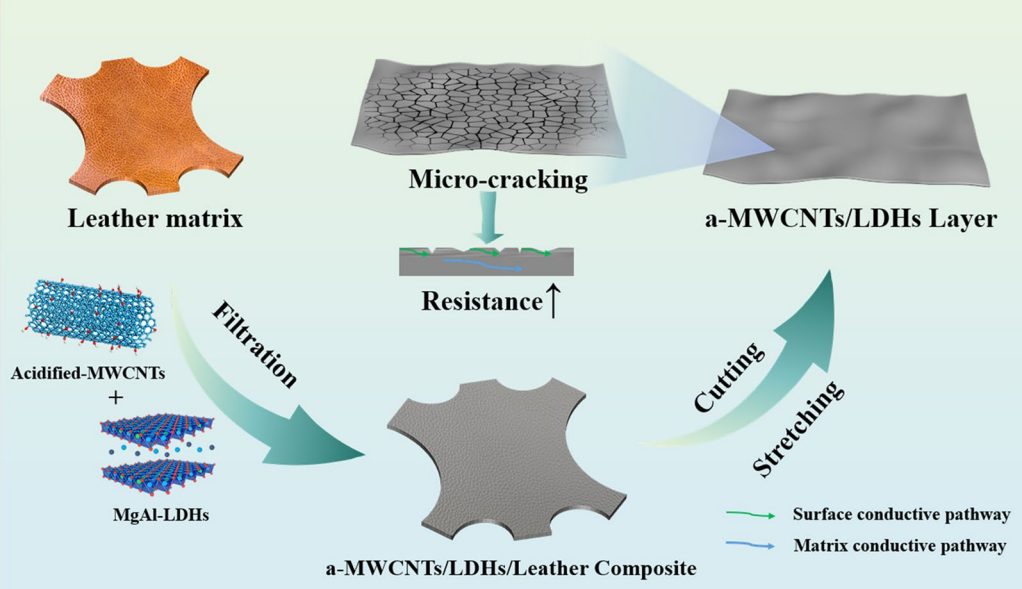

1 Introduction

Flexible strain sensors, due to their unique function to sense external stimuli by converting deformation into electrical signals, are very attractive for new-generation intelligent electronic products, *e.g.* soft robotics, human–machine interfaces, human motion monitoring and personal health monitoring devices etc. Compared to traditional heavy and rigid strain sensors made of metal or semiconductors, flexible strain sensors based on polymers are more suitable to be assembled or integrated into wearable/portable electronic devices [1, 2]. The typical flexible strain sensors are fabricated by using different polymer substrates, *e.g.* PDMS [3–5], PI [6–9], PET [10–13], PU [14–16] and rubber [17–19] etc., to incorporate conductive materials. By doing so, when force or pressure are applied on a sensor, the strain induced conductive network deformation could be transferred into resistance change, thus rendering the sensor with piezoresistive property.

The simple fabrication method and easy signal transduction mechanism make flexible strain sensor as a promising candidate for the development of wearable electronics, yet it is still necessary to optimized its overall performance, such as sensitivity, detecting range, cycling stability and wearing experience. According to previous reports, micro/nano patterning on conductive layer can effectively improve the sensitivity of flexible strain sensors. The designed micro/nano structures include micro-pyramid array [20], micro-dome array [21] and porous network [22] etc. However, the development of such structure is complicated and expensive, so it is not an ideal method for large-scale fabrication. The other issue for currently used flexible sensor is the reluctant use of synthetic polymers. Although these polymers have excellent stretchability which is the prerequisite for large detecting range, the poor breathability and air permeability prevent the volatilization of sweat and therefore extremely affect customer comfort. Moreover, synthetic polymers are difficult to degrade, which may cause a series of environmental problems.

Leather is a naturally occurring biomass derived from animal skin, in which well aligned collagen fibers are assembled as 3-D network [23]. The good air permeability and biodegradability ensure leather as a comfortable and sustainable material that has long been used to produce shoes, clothes and other accessories. Recently, some efforts have been devoted to explore new advances of using leather as the substrate to fabricate flexible strain sensor. Zou et al. pumped and filtered acidified CNTs (a-CNTs) onto leather, and the obtained a-CNTs/leather composite was combined with the other piece of leather with fork-finger electrode arrays to fabricate a flexible wearable pressure sensor. Under a certain pressure, the change of conductive pathways of the CNTs/leather composite and the corresponding output electrical signal could be detected by the fork-finger electrodes to realize strain sensing [24]. Huo et al. prepared

a leather based strain sensor with carbon black modified collagen clusters as the conductive layer, on which Kirigami is employed to create cracking structures. Such sensor is capable to detect bending angles from − 150° to 150°, with considerable sensitivity (GF = 21.49) and good cycling stability [25]. Zheng and co-workers designed a dual-functional sensor based on two pieces of acidified carbon nanotube/leather composites. Since the signal transduction mechanism is vertical contact-separation mode, this sensor can only sense pressure but is not suitable for large-range strain change detection [26]. This is the current situation of leather based flexible sensor, however, the possibility of constructing microstructural conductive layer on leather substrate, for the purpose of developing high performance leather based strain sensor, is yet to be reported.

This work demonstrates a simple and scalable fabrication strategy to prepare a leather based sensor with micro-cracking conductive layer, which is used as an alternative patterning method to create microstructural conductive network. To fabricate the sensor, acidified multi-walled carbon nanotubes (a-MWCNTs)/layered double hydroxides (LDHs) suspension was filtrated onto leather to realize conductivity. Although CNTs has excellent electrical and mechanical properties and have been widely used for sensing applications [27–30], its 1-D structure will lead to a compact conductive layer due to the entanglement of CNTs, which is not suitable for high-performance sensing in a wide strain range. By blending with 2-D material, namely the layered double hydroxides (LDHs), stretching induced strain change will cause sliding between LDHs, and this will further propagate micro-crackings on the a-MWCNTs/LDHs conductive layer. The as prepared a-MWCNTs/LDHs/leather strain sensor had dramatically improved sensitivity (GF of 7238.92), wide detecting range (60%), fast response (tensile response time of 270 ms), good stability and repeatability. The sensor could monitor full-range human motions, including large-scale strain (fingers bending, walking, running, jumping, etc.) and small-scale strain (swallowing, bulging cheeks and opening mouth) change. Besides, the introduction of LDHs also rendered the sensor with good flame retardancy and eliminate the risk of electronic fire. These features enabled the sensor as a promising wearable electronic device for human motion detection and health monitoring.

2 Experimental section

2.1 Materials

The MWCNTs was purchased from Chinese Academy of Sciences Chengdu Organic Chemistry Co., Ltd. Vanadium(III) Chloride (VCl_3) was purchased from Shanghai Dingxian Biological Technology Co., Ltd. (Shanghai, China). Urea (H_2NCONH_2) and magnesium nitrate hexahydrate ($Mg(NO_3)_2{\cdot}6H_2O$) were obtained from Tianjin Kemiou Chemical Reagent Co., Ltd. (Tianjin, China). Aluminum nitrate nonahydrate ($Al(NO_3)_3{\cdot}9H_2O$) was provided by Damao Chemical Reagent Factory (Tianjin, China). Concentrated sulfuric acid was supplied by Sinopharm Chemical Reagent Co., Ltd. Concentrated nitric acid was purchased from Gu'an County Tang Da Chemical Plant. All chemicals were used without further purification.The leather is made from sheepskin that has undergone chrome tanning and post tanning procedures from New Jin Xin Leather Co.

2.2 Preparation of a-MWCNTs

1 g of MWCNTs powder was added to 250 mL three-mouth flask, then 67.5 mL of concentrated sulfuric acid was poured into the three-mouth flask, and mechanically stirred for a period of time. Then 22.5 mL of concentrated nitric acid was added slowly, and reflux was performed at 50 ℃ for 2 h. The dispersion obtained was washed with a large amount of DI water to the filtrate pH = 7, and the filter cake was vacuum-dried at 60 ℃ to obtain a-MWCNTs.

2.3 Preparation of a-MWCNTs/LDHs suspensions

The MgAl-LDHs and MgAlV-LDHs were prepared in the same way as in our previous article [31]. a-MWCNTs/LDHs suspensions were obtained by using the physical blending method. In details, 0.05 g of a-MWCNTs was dispersed in 50 mL of deionized water by ultrasound, and a certain amount of LDHs was added. The mass ratios of a-MWCNTs to LDHs are 1:0.08, 1:0.12 and 1:0.24 in the a-MWCNTs/LDHs suspensions. After 10 min of ultrasonication, a-MWCNTs/MgAl-LDHs and a-MWCNTs/MgAlV-LDHs suspensions were stored for subsequent use.

2.4 Preparation of the a-MWCNTs/LDHs/Leather Sensors

A-MWCNTs/LDHs were combined with leather substrate (sheepskin) via vacuum filtration as follows. The leather was cut into round leather with a diameter of 100 mm to filter 50 mL of a-MWCNTs/LDHs suspension, and then was dried at 60 °C. Finally, A-MWCNTs/LDHs/leather composites were cut into rectangular strips (40×10 mm^2) and copper tape as electrodes was fixed at both ends of composites with a distance of 20 mm between the two electrodes.

2.5 Characterization

The morphology of MgAl-LDHs, MgAlV-LDHs, surface of a-MWCNTs/MgAl-LDHs/leather, surface of a-MWCNTs/MgAlV-LDHs/leather and carbon layers of all samples was observed under a Hitachi S4800 scanning

electron microscope (SEM) with an acceleration voltage of 5 kV. All samples were sprayed with gold coating for 60 s before test. The morphology of MWCNTs and a-MWCNTs was captured by a FEI Tecnai G2 F20 transmission electron microscope (TEM) along with an acceleration voltage of 200 kV. X-ray powder diffraction (XRD) patterns were conducted on a Bruker D8 Advance diffractometer with a Cu Kα radiation. Data were obtained by scanning from 5° to 70° at the scanning speed of 7°/min. A Bruker Vertex70 Fourier transform infrared spectrometry (FTIR) was used to characterize interaction between a-MWCNTs, a-MWCNTs/LDHs hybrid materials and leather. The spectra ranging of 500–4000 cm^{-1} were obtained. The sensing data was obtained from the Digital Source-meter (keithley 2450 Series). The flame retardant property was tested by CZF-4 50W vertical combustion tester.

3 Results and discussion

3.1 Fabrication of a-MWCNTs/LDHs/leather composite sensor

The fabrication process is illustrated in Fig. 1. In order to improve the dispersion of MWCNTs in water, MWCNTs were modified by concentrated sulfuric acid and concentrated nitric acid. The acid treated multi-walled carbon nanotubes (a-MWCNTs) can be evenly dispersed in water because the strong oxidation agents resulted a large number of hydrophilic groups (-COOH and –OH) on MWCNTs. Then two types of LDHs, namely, MgAl-LDHs and MgAlV-LDHs were added to a-MWCNTs aqueous dispersion. Each type of LDHs was mixed with the a-MWCNTs aqueous dispersion by ultrasonication to make sure the negatively charged a-MWCNTs and the positively charged LDHs could form a hybrid material by electrostatic interactions (Additional file 1: Table S1). Finally, conductive a-MWCNTs/MgAl-LDHs and a-MWCNTs/MgAlV-LDHs hybrid materials were applied to leather via vacuum filtration, and the resulted composites were then assembled with electrode as leather-based sensors.

3.2 Morphologies and structures of a-MWCNTs, LDHs, a-MWCNTs/LDHs and a-MWCNTs/LDHs/leather

Raman spectra proved that MWCNTs were successfully modified (Additional file 1: Figure S1). The morphology before and after the modification of MWCNTs was characterized by TEM. The MWCNTs before modification (Fig. 2a) were entangled one-dimensional materials, and their diameters are between 20 and 35 nm. In comparison, the diameter (45 nm-70 nm) of the modified a-MWCNTs (Fig. 2b) were larger than MWCNTs before modification. This is probably due to the fact that the a-MWCNTs contained a large number of –COOH and –OH, and the hydrogen bonding between them could dramatically change the morphology. MgAl-LDHs and MgAlV-LDHs were prepared by hydrothermal methods

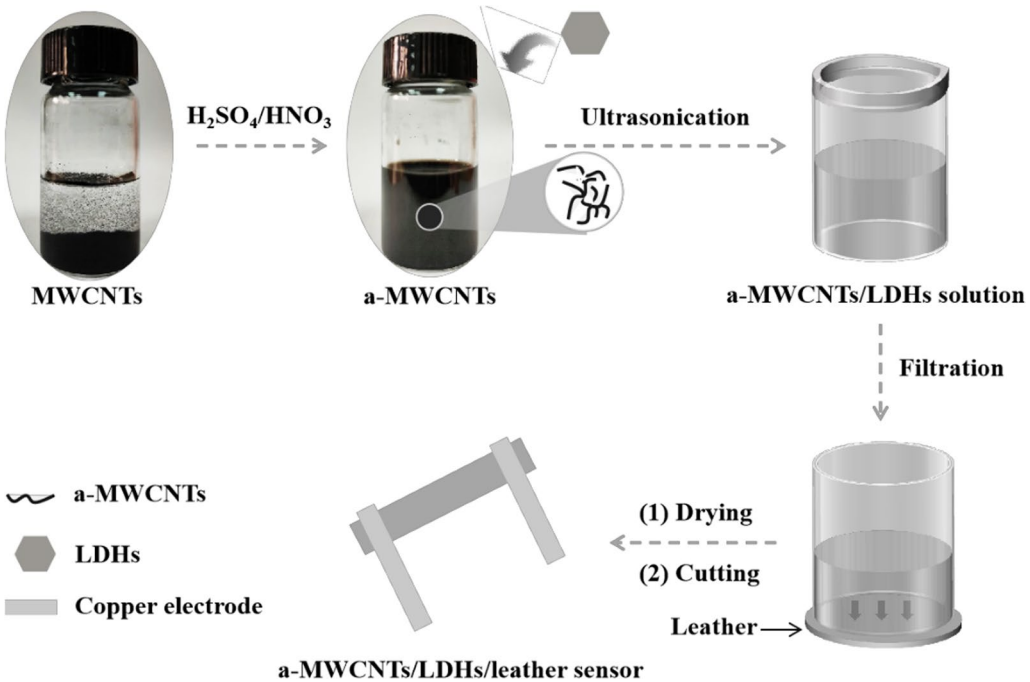

Fig. 1 Schematic illustration of preparation process of a-MWCNTs/LDHs/leather sensor

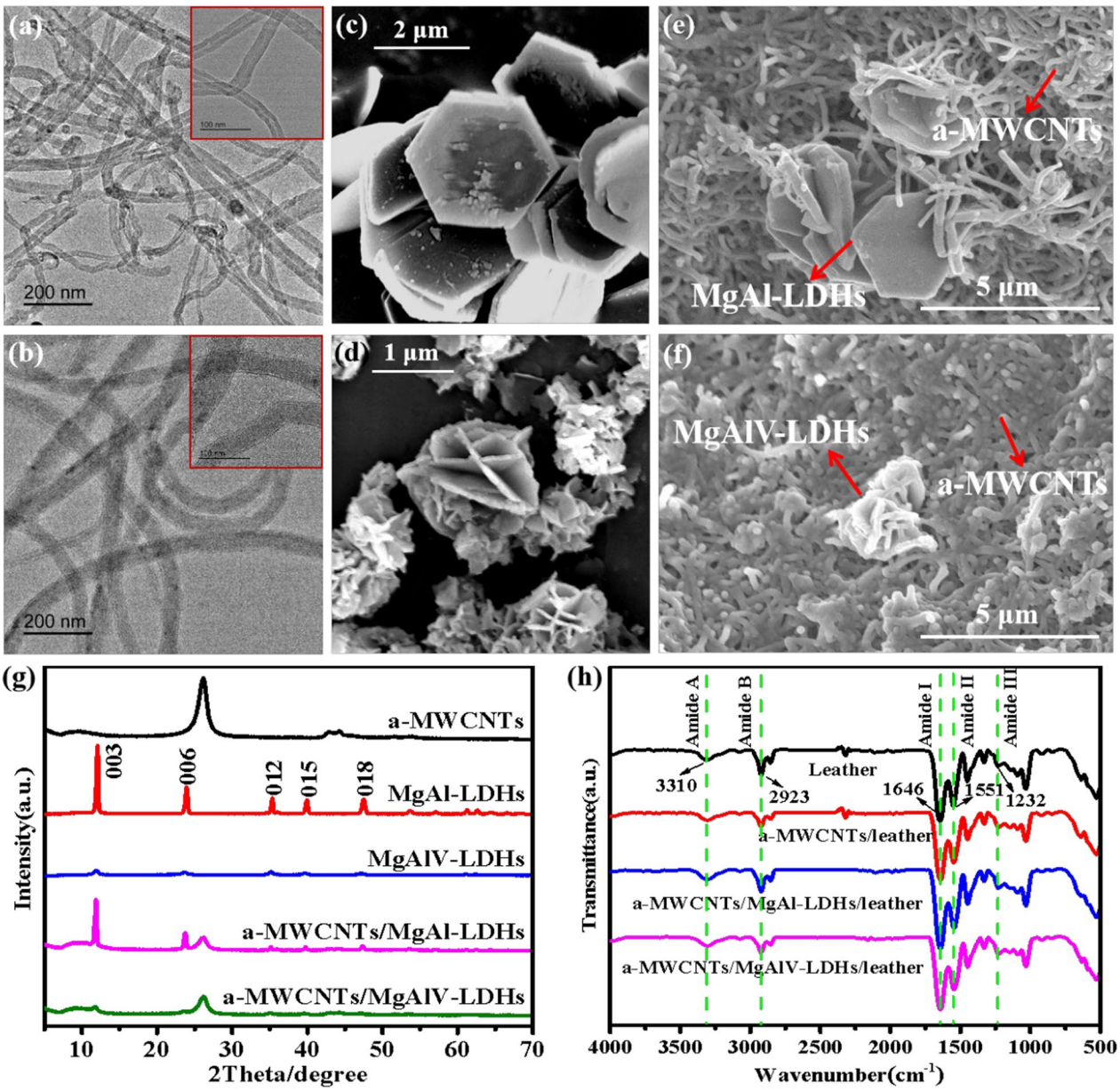

Fig. 2 TEM images of **a** MWCNTs and **b** a-MWCNTs. The inset sections are local magnified views. SEM images of **c** MgAl-LDHs, **d** MgAlV-LDHs, **e** surface of a-MWCNTs/MgAl-LDHs/leather and **f** surface of a-MWCNTs/MgAlV-LDHs/leather. **g** XRD patterns of a-MWCNTs, LDHs and a-MWCNTs/LDHs. **h** FT-IR spectra of leather, a-MWCNTs/leather, a-MWCNTs/MgAl-LDHs/leather and a-MWCNTs/MgAlV-LDHs/leather

as reported in our previous work [30]. The successful preparation of two types of LDHs was confirmed by using SEM–EDS. As shown in Additional file 1: Figure S2, MgAl-LDHs were composed of Mg element, Al element, C element and O element, while MgAlV-LDHs were composed of Mg element, Al element, V element, C element and O element, indicating that V element was successfully doped. The morphology of MgAl-LDHs and MgAlV-LDHs were shown in Fig. 2c, d. The size of the LDHs pieces was reduced from ~ 2 μm to less than 1 μm due to the doping of V^{3+}, and converted the morphology from hexagonal structure (Fig. 2c, MgAl-LDHs) to flower-like clusters (Fig. 2d, MgAlV-LDHs). The size of MgAl-LDHs and MgAlV-LDHs determines their distribution on leather substrates. As can be seen from the SEM images (Fig. 2e, f), the surface of a-MWCNTs/MgAl-LDHs/leather loaded with large amount of a-MWCNTs and hexagonal MgAl-LDHs pieces (Fig. 2e),

while flower-like MgAlV-LDHs were disassembled and only those larger than 1 μm were found on the surface of the a-MWCNTs/MgAlV-LDHs/leather composite (Fig. 2f). Smaller MgAlV-LDHs less than 1 μm were expected to enter the interior of the leather during the vacuum filtration process. This result was further confirmed by the elemental distribution of cross-sections of a-MWCNTs/MgAl-LDHs/leather and a-MWCNTs/MgAlV-LDHs/leather composites (Additional file 1: Figure S3). The grain side (top) of a-MWCNTs/MgAl-LDHs/leather composite was rich in Mg elements and Al elements, while in the interior of the leather substrate, there was less content of Mg elements and Al elements (Additional file 1: Figure S3a). This was because the pore size of leather substrate was ~ 1 μm, so large sized MgAl-LDHs were difficult to penetrate into the deep areas of leather. In contrast, the grain side (top) of a-MWCNTs/MgAlV-LDHs/leather composite was rich in Mg, Al and V elements, but unlike a-MWCNTs/MgAl-LDHs/leather composite, Mg, Al and V elements were evenly distributed in the leather matrix (Additional file 1: Figure S3b), which was because MgAlV-LDHs pieces (less than 1 μm) were smaller than pore size of leather and can easily penetrate into the leather matrix through vacuum filtration.

Figure 2g shows XRD spectra of a-MWCNTs, LDHs and a-MWCNTs/LDHs. The sharp peak at 26° is related to the (002) reflection plane of a-MWCNTs with the lattice spacing of 0.342 nm [32]. MgAl-LDHs and MgAlV-LDHs have diffraction peaks at 2θ = 12.08°, 23.95°, 35.40°, 40.04° and 47.62°, corresponding to (003), (006), (012), (015) and (018) reflection plane of LDHs respectively. This result confirms that the crystal structure of V^{3+} doped MgAlV-LDHs is similar to undoped MgAl-LDHs. According to Bragg's law $n\lambda = 2d\sin\theta$ (n is the integer, λ is the wavelength of the X-radiation, d is the lattice spacing, θ is the Bragg diffraction angle), it can be calculated that the d(003) of MgAl-LDHs and MgAlV-LDHs were 0.75 nm and 0.76 nm, respectively. Given the thickness of the LDHs pieces was 0.48 nm, the size of the anions between the LDHs layers was determined as ~ 0.27 nm, which matched the size of CO_3^{2-}, thereby confirming that the obtained MgAl-LDHs and MgAlV-LDHs are all CO_3^{2-} intercalated. However, it is obvious the crystallinity of MgAlV-LDHs decreased compared with MgAl-LDHs, suggesting the addition of V^{3+} probably inhibited the growth of crystal thus reducing the size of LDHs pieces.. The result had a good agreement with the morphologies shown in Fig. 2c, d. The diffraction peaks of a-MWCNTs and LDHs exist simultaneously in a-MWCNTs/MgAl-LDHs and a-MWCNTs/MgAlV-LDHs hybrid materials, indicating the co-existence of the two types of materials in the mixtures. To explore the interaction of a-MWCNTs and a-MWCNTs/LDHs with leather, Fig. 2h shows the Fourier transform infrared (FTIR) spectra of leather, a-MWCNTs/leather, a-MWCNTs/MgAl-LDHs/leather and a-MWCNTs/MgAlV-LDHs/leather, respectively. The leather has a special triple-helical structure and exhibited a characteristic amide band in the infrared spectrum. These features include the stretching vibration of N–H and hydrogen bond association peak at 3310 cm^{-1} for amide A band, the stretching vibration of N–H at 2923 cm^{-1} for amide B band, the stretching vibration of C = O at 1646 cm^{-1} for amide I band, the bending vibration of N–H and the stretching vibration of C-N at 1551 cm^{-1} for amide II band, the bending vibration of N–H, the stretching vibration of C-N and wagging vibration of CH2 at 1232 cm^{-1} for amide III band [33, 34].As presented in Fig. 2h, these typical amide bands did not shift according to the introduction of a-MWCNTs or a-MWCNTs/LDHs, suggesting that incorporation of the a-MWCNTs or a-MWCNTs/LDHs with leather did not destroy the triple-helical conformation of collagen fibers in leather. Moreover, it was also confirmed that there was no electrostatic interaction nor hydrogen bonding established between a-MWCNTs and leather [35], which may be because a-MWCNTs and collagen fibers in leather only entangled with each other and they were difficult to interact at the molecular level due to complex spatial structures.

3.3 Sensing Performance of a-MWCNTs/LDHs/Leather Composite Sensors

To explore the factors that affect sensing performance, suspensions with various a-MWCNTs contents (0.2 g/L, 1 g/L and 2 g/L)were employed for filtration to load different amounts of conductive materials onto leather based sensors. Additional file 1: Figure S4 shows the sensitivity of a-MWCNTs/leather sensors prepared at a-MWCNTs concentrations of 0.2 g/L, 1 g/L and 2 g/L. Here, the sensitivity of the sensors is expressed by gauge factor (GF), which can be calculated using the following equation:

$$GF = (\Delta R/R_0)/\Delta\varepsilon \quad (1)$$

where ΔR represents the change in resistance before and after the strain is applied, R0 refers to the initial resistance and Δε is the change in strain before and after stretching. Significantly, the sensitivity of a-MWCNTs/leather composite was the highest and the strain range was also the largest when the concentration of a-MWCNTs was 1 g/L. Based on this, a-MWCNTs with a concentration of 1 g/L were selected to prepare the leather based strain sensor. Figure 3a–f show the sensitivity test result of a-MWCNTs/LDHs/leather prepared with different contents of LDHs and 1 g/L of a-MWCNTs. It is clear that the sensing performance of the obtained

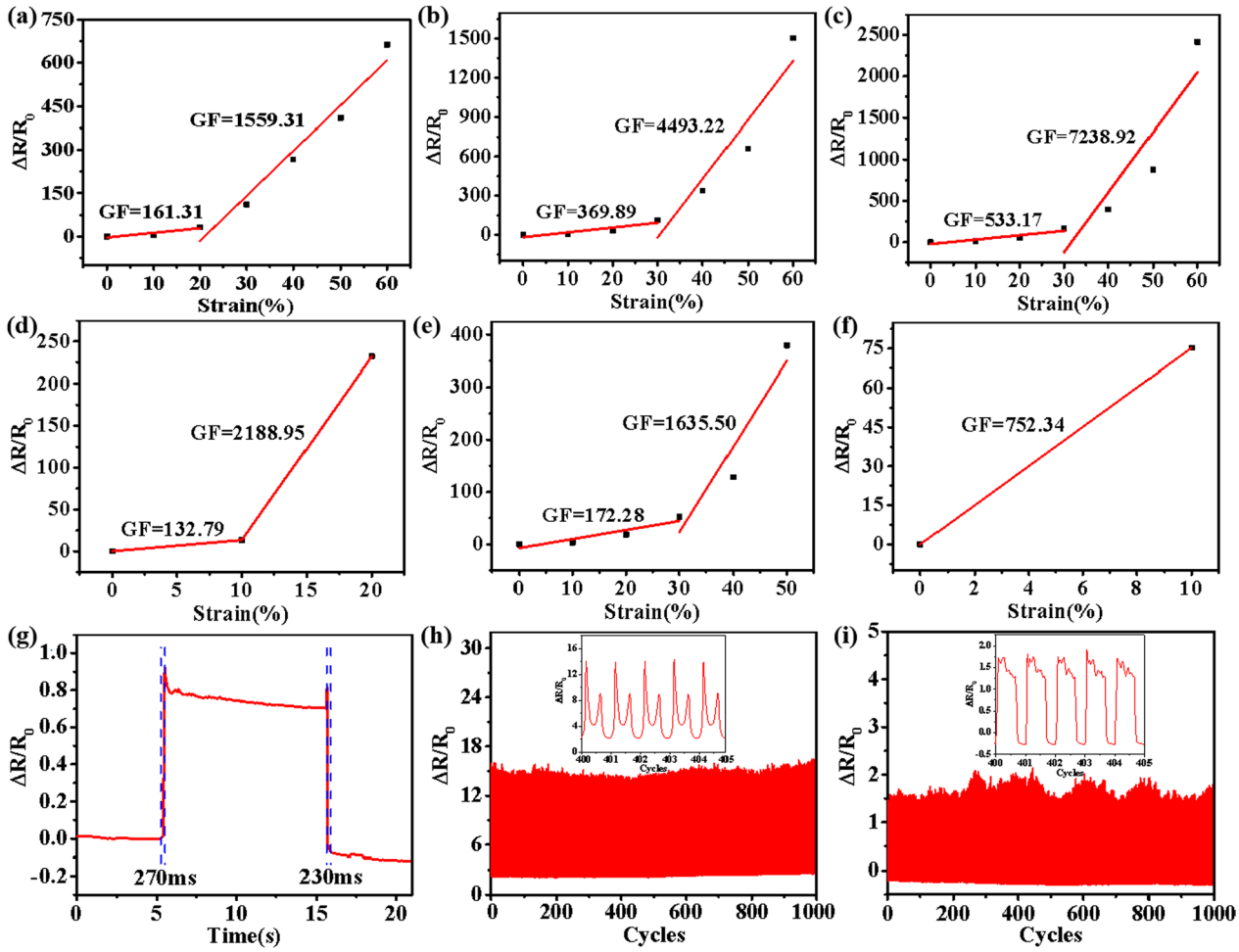

Fig. 3 Gauge factors of a-MWCNTs/MgAl-LDHs/leather sensors with **a** 8 wt.%, **b** 12 wt.% and **c** 24 wt.% of MgAl-LDHs. Gauge factors of a-MWCNTs/MgAlV-LDHs/leather sensors with **d** 8 wt.%, **e** 12 wt.% and **f** 24 wt.% of MgAlV-LDHs. **g** Tensile response time of a-MWCNTs/MgAl-LDHs/leather sensor (24 wt.% of MgAl-LDHs). Sensing stability test of the a-MWCNTs/MgAl-LDHs/leather sensor(24 wt.% of MgAl-LDHs) show the relative resistance changes under **h** cyclic stretching ε = 10% with a frequency of 0.25 Hz over 1000 cycles and **i** repeated compression up to 1000 cycles under 70 kPa with a frequency of 1 Hz

a-MWCNTs/MgAl-LDHs/leather and a-MWCNTs/MgAlV-LDHs/leather was different according to the type as well as the loading amount of LDHs. For all a-MWCNTs/MgAl-LDHs/leather sensors (Fig. 3a–c), ΔR/R0 had a linear response relationship with strain at two stages, that is, at beginning stage of low strain range, the GF was smaller than that in higher strain range. The mechanism underlying is that the a-MWCNTs/MgAl-LDHs conductive layer underwent slight deformation when strain was less than 30%, and the corresponding sensitivity values (GF) were all under 1000. After then when strain increased over 30%, the sliding between LDHs caused the occurrence of micro-crackings on the conductive layer, leading to much higher sensitivity. To verify the mechanism, the surface morphology change of the conductive layer was studied by SEM. Additional file 1: Figure S5 shows the surface (grain side) of a representative sensor, a-MWCNTs/MgAl-LDHs/leather with 24 wt.% LDHs loading, on which micro-cracking structure was observed at 40% strain and then propagated with increased strain (60%). Also, as displayed in Fig. 3a–c, the sensitivity of a-MWCNTs/MgAl-LDHs/leather sensors gradually increased with the increasing introduction of MgAl-LDHs. The highest GF of 7238.92 in the 30%-60% strain range was found from a-MWCNTs/MgAl-LDHs/leather sensor with 24 wt.% MgAl-LDHs. In contrast, for all a-MWCNTs/MgAlV-LDHs/leather sensors, their sensitivity tended to decrease with more introduction of MgAlV-LDHs, as depicted in Fig. 3d–f. It is worth to note that the effective strain range of a-MWCNTs/

MgAlV-LDHs/leather with 24 wt.% MgAlV-LDHs was only 10% (Fig. 3f), suggesting the structure of the conductive layer based on MgAlV-LDHs was not capable to detect large strain change. The relatively poor performance of a-MWCNTs/MgAlV-LDHs/leather sensors could be attributed to smaller size and various shapes of MgAlV-LDHs, which were assembled as a more compact conductive layer and the sliding between LDHs was prohibited according to strain change. Shown in Additional file 1: Figure S5b is the representative a-MWCNTs/MgAlV-LDHs/leather sensor with 8 wt.% of LDHs. Even though the tiny loading amount, MgAlV-LDHs still form a dense and rigid percolated layer on the surface, as the result the conductive layer could not withstand stretching and was completely damaged once strain reached 30%. So it is reasonable to conclude that the appropriate selection of LDHs is the key factor to achieve good sensing performance. Specifically, with larger MgAl-LDHs which were all hexagonally shaped, the propagation of micro-crackings is controlled as the LDHs were loosely overlapped each other and the sliding between them was allowed. However, with smaller MgAlV-LDHs the occurrence of micro-crackings was not controllable, thus the severe crackings may block the surface conductive pathway and therefore made the sensor lose it function (Additional file 1: Figure S6). This conclusion was consistent with the results of the sensitivity tests. Therefore, the strain range and sensitivity of a-MWCNTs/MgAl-LDHs/leather sensor with 24 wt.% LDHs was more suitable for human motion detection. The excellent performance of the sensor was achieved due to synergistic effect between the 1-D conductive materials, a-MWCNTs, and the 2-D LDHs. In comparison with other piezoresistive strain sensors based on synthetic polymers (Additional file 1: Table S2) [36–40], our a-MWCNTs/MgAl-LDHs/leather sensor demonstrated dramatically improved sensitivity. The sliding between LDHs lubricated the movement of a-MWCNTs, ensuring the conductive layer can withstand large strain change so as to increase the detecting range. While the micro-crackings arisen therefrom could enhanced the sensitivity of the sensor.

As for a sensor, response time is another important metric for performance evaluation. Represented in Fig. 3g is the resistance change of a-MWCNTs/MgAl-LDHs/leather sensor in stretching mode and the response time of 270 ms is a considerable value that can meet the requirements of real-time of human motion detection (Additional file 1: Figure S7). Furthermore, the a-MWCNTs/MgAl-LDHs/leather sensor also exhibited excellent sensing stability and recyclability in both stretching (Fig. 3h) and compressive (Fig. 3i) modes. Specifically, $\Delta R/R_0$ had periodical changes during cyclic stretching of $\varepsilon = 10\%$ with a frequency of 0.25 Hz over 1000 cycles (Fig. 3h), and the repeating pattern of output signal confirmed good stretching durability and reproducibility of the sensor. For compression test, in order to ensure sufficient bending, the sensor was combined with a PDMS substrate, and then stimuli of 70 kPa was applied to the sensor by using a mechanical slider for 1000 times. Obviously in Fig. 3i, $\Delta R/R_0$ also presented periodical changes during cyclic compression, however, due to the relatively narrow strain generated by bending, $\Delta R/R_0$ was only ~ 1.7 in the compression state (Fig. 3i) while $\Delta R/R_0$ can reach ~ 14 in stretching mode (Fig. 3h).

The outstanding flexibility, sensitivity, stability, and durability make the a-MWCNTs/MgAl-LDHs/leather sensor as a good candidate for real-time monitoring of human movements. As shown in Fig. 4a, the sensor can output corresponding electrical signals according to different bending angles (0°, 30°, 90°) of index finger. Figure 4b, c illustrate relative resistance changes when the sensor was used for monitoring the bending of the elbow and wrist, respectively. The $\Delta R/R_0$ value increased when the joint was bent, but returned to the initial value when the arm was straightened. When the sensor was used as a pedometer in compression mode, the intensity of human movement can be recognized. As shown in Fig. 4d–f, when the sensor was used for monitoring normal human walking, normal running and jumping, the electrical signal showed different characteristics in terms of peak-intensity, width, and frequency etc. For example, a series of wide peaks were generated during walking, while narrower and sharper peaks can be observed during running and jumping. In addition, other information such as the frequency of walking can be obtained from the response curve. Besides it can be used to monitor vigorous limb movements, the sensor can detect subtle physiological activities as well. As displayed in Fig. 4g, when the sensor was fixed to throat of wearer, it could record signals generated by swallowing. When the wearer repeatedly puffed up his cheeks and opened his mouth, the $\Delta R/R_0$ value changed accordingly (Fig. 4h, i). In addition, when these actions were repeated, similar waveforms would appear in the response curve, indicating that a-MWCNTs/MgAl-LDHs/leather sensor has good stability and repeatability.

3.4 Flame retardant properties of a-MWCNTs/LDHs/leather composites

LDHs can be used as flame retardants for polymer composites, as expressed in previous reports [41, 42]. Table 1 and Additional file 1: Figure S8 show the vertical burning test results for leather, a-MWCNTs/leather and a-MWCNTs/LDHs/leather. Compared with leather and a-MWCNTs/leather, burning time, damaged length and mass loss rate of a-MWCNTs/MgAl-LDHs/leather

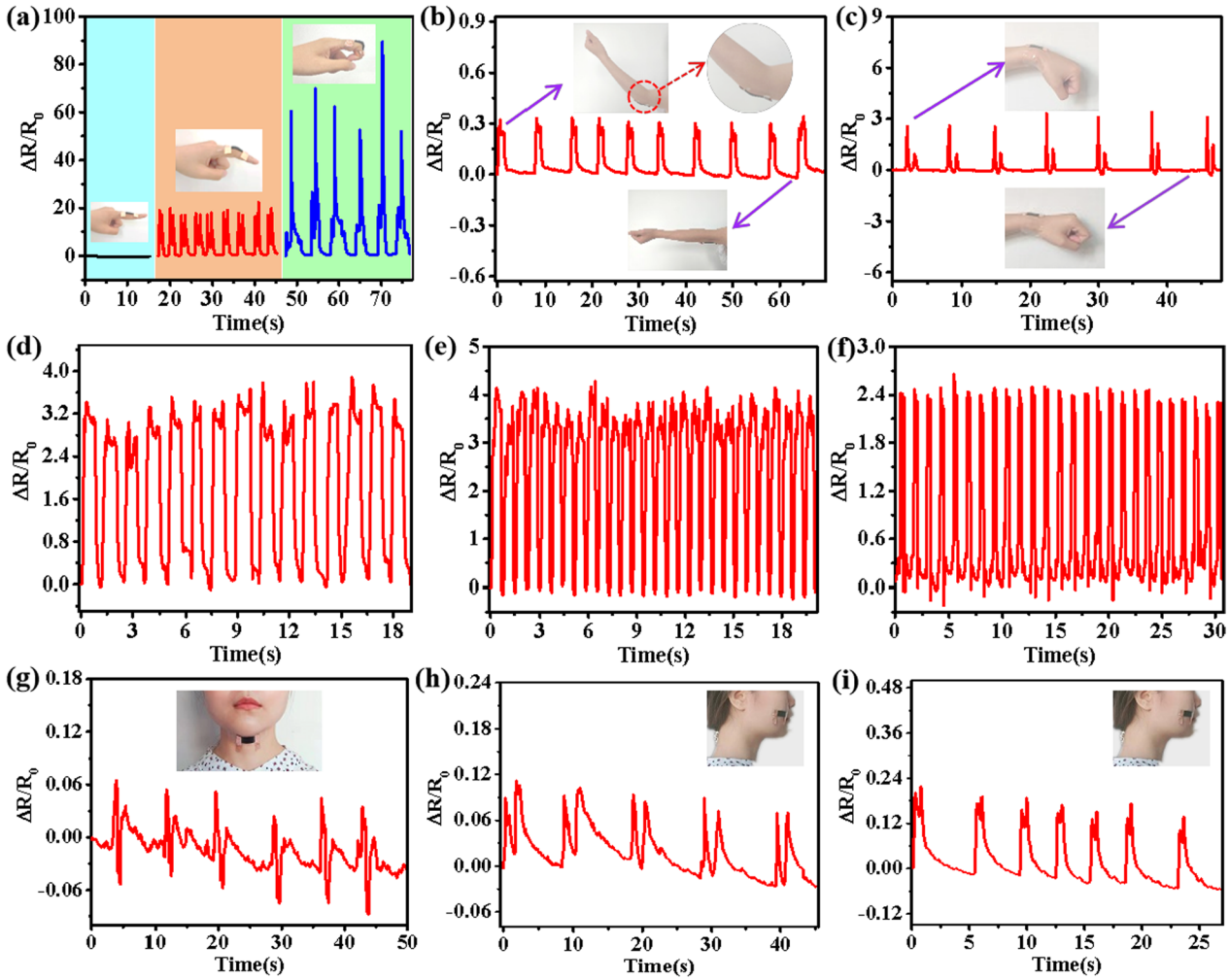

Fig. 4 Real-time human motion detection by using a-MWCNTs/MgAl-LDHs/leather sensor with 24 wt.% LDHs. Relative resistance changes corresponding to different joint movements: **a** index finger, **b** elbow, **c** wrist; Relative resistance changes during **d** normal walking, **e** normal running and **f** jumping processes; Responsive curves of the sensor when the wearer **g** swallowed, **h** puffed out cheek and **i** opened the mouth. The illustration in (**g**–**i**) shows sensors attached to the throat and cheek, respectively

and a-MWCNTs/MgAlV-LDHs/leather composite were reduced (Table 1), illustrating that flame retardant properties have been improved due to the introduction of MgAl-LDHs and MgAlV-LDHs. In order to explore the underlying mechanism for the improvement of the flame retardant property of leather, the morphologies of leather, a-MWCNTs/MgAl-LDHs/leather and a-MWCNTs/MgAlV-LDHs/leather composites after combustion were observed by SEM. As shown in Fig. 5a, the leather residues after combustion test had a loose and porous structure, so it was not capable to prevent transfer of heat and oxygen during combustion. In contrast, a-MWCNTs/MgAl-LDHs/leather and a-MWCNTs/MgAlV-LDHs/leather both formed a dense carbonized fiber structure with no porous structure on the surface (Fig. 5b, c). The morphology difference of residues is the result of thermal decomposition of MgAl-LDHs and MgAlV-LDHs, which resulted in the formation of carbon and metal oxides. When combined with collagen fibers, they can act as a barrier to isolate heat flow and delay oxygen supply. Furthermore, the synergistic flame retardant effect of a-MWCNTs and LDHs was helpful for improving flame retardant properties of leather as well. Figure 5d–e are infrared images of a-MWCNTs/MgAl-LDHs/leather and a-MWCNTs/MgAlV-LDHs/leather sensors connected with 2 V power supply at room temperature for 10 min. For each type of the sensors, LDHs contents were 8 wt.%, 12 wt.% and 24 wt.% from top to bottom. The temperature of a-MWCNTs/MgAl-LDHs/leather and a-MWCNTs/MgAlV-LDHs/

Table 1 Vertical burning test of leather and leather based composites

Sample	After flame time (s)	The length of charring (mm)	Mass loss rate (%)
Leather	58	76	60.2
a-MWCNTs/leather	55	73	59.3
a-MWCNTs/MgAl-LDHs-8%/leather	41	50	43.3
a-MWCNTs/MgAl-LDHs-12%/leather	34	44	39.5
a-MWCNTs/MgAl-LDHs-24%/leather	37	48	42.6
a-MWCNTs/MgAlV-LDHs-8%/leather	33	48	39.8
a-MWCNTs/MgAlV-LDHs-12%/leather	33	41	34.2
a-MWCNTs/MgAlV-LDHs-24%/leather	35	43	38.4

leather, no matter how much LDHs were loaded, did not change significantly. This result suggested that the electrothermal efficiency of prepared sensor was quite low, thus ensuring the safety of use.

3.5 Hygienic and mechanical properties of a-MWCNTs/LDHs/leather composites

To verify if the introduced a-MWCNTs/LDHs hybrid materials would affect the breathability, pure leather, a-MWCNTs/MgAl-LDHs/leather and a-MWCNTs/MgAlV-LDHs/leather composites were fixed on an empty beaker, respectively, as shown in Additional file 1: Figure S9. Then, 20 mL of concentrated HCl was quickly added to the beaker, and methyl orange droplets were used as indicators on the surfaces of the samples to test the air flow rate. It is worth noting that the droplets on the surface of the pure leather samples turned into red within 15 s, while a-MWCNTs/MgAl-LDHs/leather and a-MWCNTs/MgAlV-LDHs/leather composites samples turned into completely red within 40 and 60 s, respectively. This result indicate that the introduction of a-MWCNTs/LDHs may partially fill in the porous structure in leather substrate and obstruct the air flow pathways, but breathability is not eliminated. In addition, as discussed earlier, there were more MgAlV-LDHs penetrated into leather substate due to their smaller size (Fig. 2 and Additional file 1: S3). This could be the reason that the corresponding a-MWCNTs/MgAlV-LDHs/leather composite had reduced air permeability than its counterpart, a-MWCNTs/MgAl-LDHs/leather composite, as evidenced by

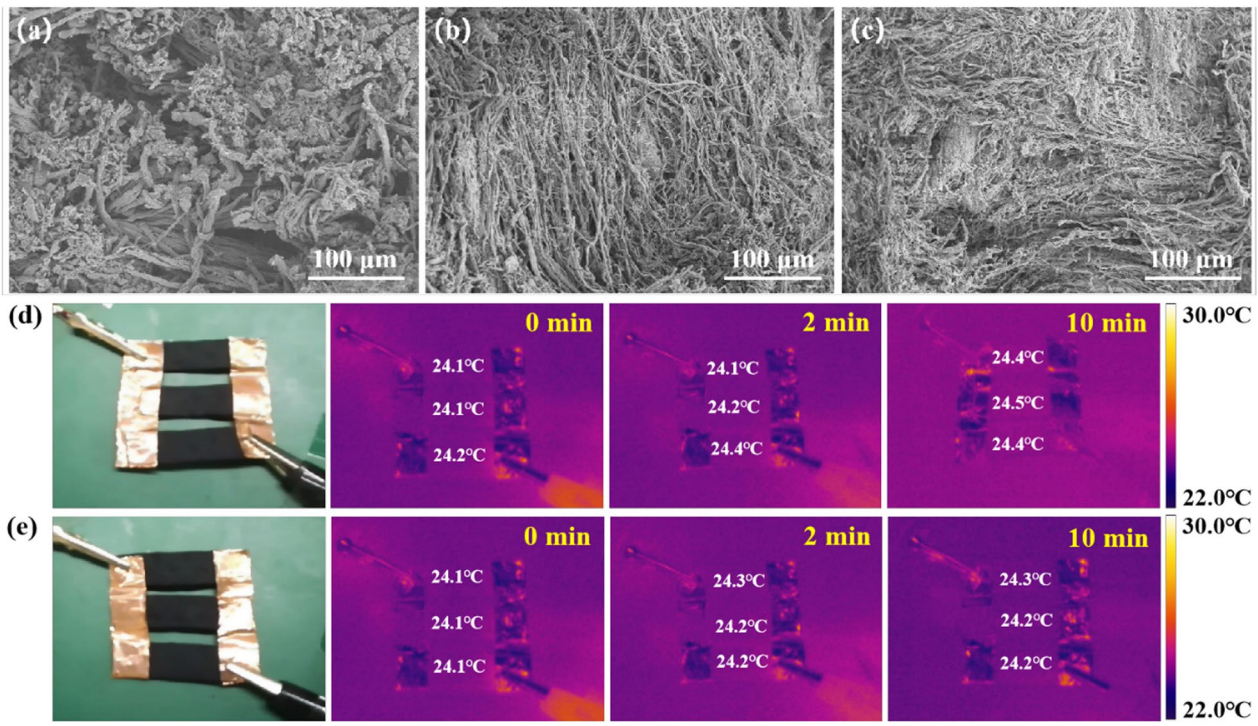

Fig. 5 SEM images of the morphology of **a** leather, **b** a-MWCNTs/MgAl-LDHs/leather and **c** a-MWCNTs/MgAlV-LDHs/leather composites after burning test; Infrared images of **d** a-MWCNTs/MgAl-LDHs/leather and **e** a-MWCNTs/MgAlV-LDHs/leather connected with 2 V power supply at room temperature for 10 min. LDHs contents in the samples were 8 wt.%, 12 wt.% and 24 wt.% from top to bottom

the longer time need for indicator droplets to change the color (Additional file 1: Figure S9). The mechanical strength of the leather was illustrated by determining the stress–strain curve of the leather. From the result it is clear the maximum elongation ratio of the leather can reach up to ~ 90% (Additional file 1: Figure S10).

4 Conclusion

In conclusion, a-MWCNTs/MgAl-LDHs/leather composite sensor with excellent sensing ability, flame-retardant performance and wearable experience was successfully fabricated through a simple vacuum filtration method. Being benefited from the unique 2-D structure of LDHs, the propagation of micro-cracking structures was allowed on percolated a-MWCNTs/MgAl-LDHs conductive layer, resulting a dramatically enhanced sensitivity (GF of 7238.92 at strain 30–60%) and a considerable overall performance. The fabricated strain sensor was employed for practical application, exhibiting excellent performance for the detection of subtle physiological activities and vigorous limb movements. This work provided a concept of using controlled micro-carckings as an easy and low-cost method to construct microstructural conductive network in order to achieve high performance strain sensors. The development of high performance leather based sensor is also expected to bring additional value to the traditional leather products, and leading to the emergence of new flexible electronics with good wearing experience.

Supplementary Information

The online version contains supplementary material available at https://doi.org/10.1186/s42825-023-00134-6.

Additional file 1. Supporting information for the article. Supplementary tables and figures.

Acknowledgements
We would like to thank Wenbo Zhang from Shaanxi University of Science and Technology Shaanxi Collaborative Innovation Center of Industrial Auxiliary Chemistry and Technology for his technical assistance with SEM.

Author contributions
JM and YZ devised this study. ST performed most of the experiments and analyses, and wrote the manuscript under the supervision of JM and YZ. TZ, YZ and ST participated in the discussion of the mechanism of this study. ZC revised the logical and grammatical aspects of this manuscript. All authors reviewed the study results, revised the manuscript and approved the final version of the manuscript.

Funding
This work was supported by the National Natural Science Foundation of China (No. 51903143) and Special Foundation for Science and Technology Major Plan of Xianyang (No. 2018k01-46).

Availability of data and materials
All data generated or analyzed during this study are included in this published article [and its supplementary information files].

Declarations

Competing interests
Jianzhong Ma is a member of the editorial board of Collagen and Leather, and was not involved in the editorial review, or the decision to publish this article. All authors declare that there are no competing interests.

Author details
[1]College of Bioresources Chemical and Materials Engineering, Shaanxi University of Science and Technology, Xi'an 710021, China. [2]Xi'an Key Laboratory of Green Chemicals and Functional Materials, Xi'an 710021, China. [3]Materials Characterization and Fabrication Platform, Department of Chemical Engineering, University of Melbourne, Parkville, Melbourne 3010, Australia.

Received: 15 June 2023 Revised: 4 September 2023 Accepted: 11 September 2023
Published online: 22 September 2023

References

1. Lee J, Lim M, Yoon J, et al. Transparent, flexible strain sensor based on a solution-processed carbon nanotube network. ACS Appl Mater Interfaces. 2017;9(31):26279–85.
2. Zheng Y, Li Y, Li Z, et al. The effect of filler dimensionality on the electromechanical performance of polydimethylsiloxane based conductive nanocomposites for flexible strain sensors. Compos Sci Technol. 2017;139:64–73.
3. Ahuja P, Ujjain SK, Urita K, et al. Chemically and mechanically robust SWCNT based strain sensor with monotonous piezoresistive response for infrastructure monitoring. Chem Eng J. 2020;388: 124174.
4. Puneetha P, Mallem S, Lee YW, et al. Strain-controlled flexible graphene/GaN/PDMS sensors based on the piezotronic effect. ACS Appl Mater Interfaces. 2020;12(32):36660–9.
5. Tas MO, Baker MA, Masteghin MG, et al. Highly stretchable, directionally oriented carbon nanotube/PDMS conductive films with enhanced sensitivity as wearable strain sensors. ACS Appl Mater Interfaces. 2019;11(43):39560–73.
6. Chhetry A, Sharifuzzaman M, H Yoon, et al. MoS_2-decorated laser-induced graphene for a highly sensitive, hysteresis-free, and reliable piezoresistive strain sensor. ACS Appl Mater Interfaces 2019;11(25):22531–22542.
7. Jiang Y, He Q, Cai J, et al. Flexible strain sensor with tunable sensitivity via microscale electrical breakdown in graphene/polyimide thin films. ACS Appl Mater Interfaces. 2020;12(52):58317–25.
8. Li M, Guo L, Ding G, et al. Inorganic perovskite quantum dot-based strain sensors for data storage and in-sensor computing. ACS Appl Mater Interfaces. 2021;13(26):30861–73.
9. Qin Y, Peng Q, Ding Y, et al. Lightweight, superelastic, and mechanically flexible graphene/polyimide nanocomposite foam for strain sensor application. ACS Nano. 2015;9:8933–41.
10. Lee T, Choi YW, Lee G, et al. Transparent ITO mechanical crack-based pressure and strain sensor. J Mater Chem C. 2016;4:9947–53.
11. Lee Y, Bae S, Jang H, et al. Wafer-scale synthesis and transfer of graphene films. Nano Lett. 2010;10(2):490–3.
12. Qin Y, Qu M, Pan Y, et al. Fabrication, characterization and modelling of triple hierarchic PET/CB/TPU composite fibres for strain sensing. Compos A Appl Sci Manuf. 2019;129: 105724.
13. Tian H, Shu Y, Cui YL, et al. Scalable fabrication of high-performance and flexible graphene strain sensors. Nanoscale. 2013;6(2):699–705.
14. Gao Y, Guo F, Cao P, et al. Winding-locked carbon nanotubes/polymer nanofibers helical yarn for ultrastretchable conductor and strain sensor. ACS Nano. 2020;14(3):3442–50.
15. Sun H, Dai K, Zhai W, et al. A highly sensitive and stretchable yarn strain sensor for human motion tracking utilizing a wrinkle-assisted crack structure. ACS Appl Mater Interfaces. 2019;11(39):36052–62.
16. Wu YH, Liu HZ, Chen S, et al. Channel crack-designed gold@PU sponge for highly elastic piezoresistive sensor with excellent detectability. ACS Appl Mater Interfaces. 2017;9(23):20098–105.

17. Lynch PJ, Ogilvie SP, Large MJ, et al. Graphene-based printable conductors for cyclable strain sensors on elastomeric substrates. Carbon. 2020;169:25–31.
18. Wang L, Luo J, Chen Y, et al. Fluorine-free superhydrophobic and conductive rubber composite with outstanding deicing performance for highly sensitive and stretchable strain sensors. ACS Appl Mater Interfaces. 2019;11(19):17774–83.
19. Zhang Q, Pan S, Ji C, et al. A shapeable, ultra-stretchable rubber strain sensor based on carbon nanotubes and Ag flakes via melt-mixing process. J Mater Chem B. 2021;9:3502–8.
20. Choong CL, Shim MB, Lee BS, et al. Highly stretchable resistive pressure sensors using a conductive elastomeric composite on a micropyramid array. Adv Mater. 2014;26:3451–8.
21. Park J, Lee Y, Hong J, et al. Giant tunneling piezoresistance of composite elastomers with interlocked microdome arrays for ultrasensitive and multimodal electronic skins. ACS Nano. 2014;8:4689–97.
22. Pang Y, Tian H, Tao L, et al. Flexible, highly sensitive, and wearable pressure and strain sensors with graphene porous network structure. ACS Appl Mater Interfaces. 2016;8:26458–62.
23. Yang N, Ma J, Shi J, et al. Manipulate the nano-structure of layered double hydroxides via calcination for enhancing immobilization of anionic dyes on collagen fibers. J Colloid Interface Sci. 2022;610:182–93.
24. Zou B, Chen Y, Liu Y, et al. Repurposed leather with sensing capabilities for multifunctional electronic skin. Adv Sci. 2019;6(3):1801283.
25. Xie R, Hou S, Chen Y, et al. Leather-based strain sensor with hierarchical structure for motion monitoring. Adv Mater Technol. 2019;4:1900442.
26. Chen YY, Xie RJ, Zou BH, et al. CNT@leather-based electronic bidirectional pressure sensor. Sci China Technol Sci 2020;63(10).
27. Gu J, Kwon D, Ahn J, et al. Wearable strain sensor using light transmittance change of carbon nanotube embedded elastomer with microcrack. ACS Appl Mater Interfaces. 2020;12(9):10908–17.
28. Ko Y, Kim J, Vu C, et al. Ultrasensitive strain sensor based on pre-generated crack networks using Ag nanoparticles/single-walled carbon nanotube (SWCNT) hybrid fillers and a polyester woven elastic band. Sensors. 2021;21(7):2531.
29. Li Z, Qi X, Xu L, et al. Self-repairing, large linear working range shape memory carbon nanotubes/ethylene vinyl acetate fiber strain sensor for human movement monitoring. ACS Appl Mater Interfaces. 2020;12(37):42179–92.
30. Yang G, Feng X, Wang W, et al. Graphene and carbon nanotube-based high-sensitive film sensors for in-situ monitoring out-of-plane shear damage of epoxy composites. Compos B Eng. 2021;204(21): 108494.
31. Zong Y, Tan S, Ma J. Flame-retardant PEDOT: PSS/LDHs/Leather flexible strain sensor for human motion detection. Macromol Rapid Commun. 2022;43(8):2100873.
32. Tannarana M, Pataniya PM, Bhakhar SA, et al. Humidity sensor based on two-dimensional $SnSe_2$/MWCNTs nanohybrid for the online monitoring of human respiration and touchless positioning interface. ACS Sustain Chem Eng. 2020;8(33):12595–602.
33. Jose MV, Thomas V, Dean DR, et al. Fabrication and characterization of aligned nanofibrous PLGA/collagen blends as bone tissue scaffolds. Polymer. 2009;50(15):3778–85.
34. Yang N, Ma J, Shi J, et al. pH-triggered MgAlZr layered double hydroxides for modification of collagen fibers with enhanced thermal stability and UV resistance. Appl Clay Sci. 2020;198(7): 105827.
35. Andrews ME, Murali J, Muralidharan C, et al. Interaction of collagen with corilagin. Colloid Polym Sci. 2003;281(8):766–70.
36. Wang H, Zhou R, Li D, et al. High-performance foam-shaped strain sensor based on carbon nanotubes and $Ti_3C_2T_x$ MXene for the monitoring of human activities. ACS Nano. 2021;15(6):9690–700.
37. Liang B, Lin Z, Chen W, et al. Ultra-stretchable and highly sensitive strain sensor based on gradient structure carbon nanotubes. Nanoscale. 2018;10(28):13599–606.
38. Ding YR, Xue CH, Fan QQ, et al. Fabrication of superhydrophobic conductive film at air/water interface for flexible and wearable sensors. Chem Eng J. 2021;404: 126489.
39. Wang S, Xiao P, Liang Y, et al. Network cracks-based wearable strain sensors for subtle and large strain detection of human motions. J Mater Chem C. 2018;6(19):5140–7.
40. Sun X, Qin Z, Ye L, et al. Carbon nanotubes reinforced hydrogel as flexible strain sensor with high stretchability and mechanically toughness. Chem Eng J. 2020;382: 122832.
41. Li Z, Zhang J, Dufosse F, et al. Ultrafine nickel nanocatalyst-engineering of an organic layered double hydroxide towards a super-efficient fire-safe epoxy resin via interfacial catalysis. J Materi Chem A. 2018;6:8488–98.
42. Zhou K, Gao R, Qian X. Self-assembly of exfoliated molybdenum disulfide (MoS_2) nanosheets and layered double hydroxide (LDH): Towards reducing fire hazards of epoxy. J Hazard Mater. 2017;338:343–55.

Publisher's Note